THE JOURNAL OF PHYSICAL CHEMISTRY LETTERS
A JOURNAL OF THE AMERICAN CHEMICAL SOCIETY

pubs.acs.org/JPCL Letter

Rydberg Atom-Enabled Spectroscopy of Polar Molecules via Förster Resonance Energy Transfer

Sabrina Patsch, Martin Zeppenfeld, and Christiane P. Koch*

Cite This: J. Phys. Chem. Lett. 2022, 13, 10728−10733 Read Online

ACCESS | Metrics & More | Article Recommendations | Supporting Information

ABSTRACT: Non-radiative energy transfer between a Rydberg atom and a polar molecule can be controlled by a static electric field. Here, we show how to exploit this control for state-resolved, non-destructive detection and spectroscopy of the molecules, where the lineshape reflects the type of molecular transition. Using the example of ammonia, we identify the conditions for collision-mediated spectroscopy in terms of the required electric field strengths, relative velocities, and molecular densities. Rydberg atom-enabled spectroscopy is feasible with current experimental technology, providing a versatile detection method as a basic building block for applications of polar molecules in quantum technologies and chemical reaction studies.

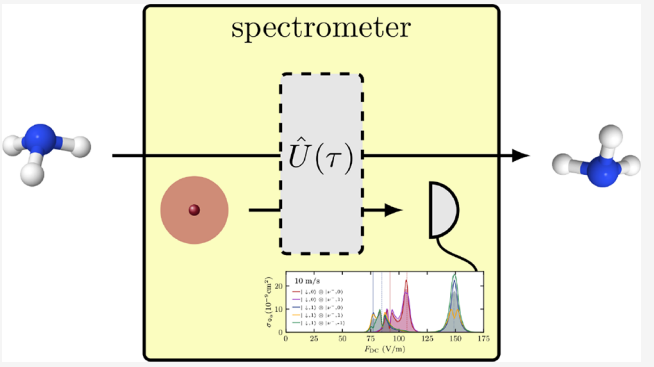

Cold polar molecules are excellent candidates for quantum control, with applications ranging from fundamental physics[1,2] and quantum information[3−5] to cold chemistry.[6] The ability to detect the molecules, ideally at the single-molecule level and in a non-destructive and state-resolved fashion, is a prerequisite to any such application. Optical detection schemes, such as laser-induced fluorescence or absorption,[7−10] are destructive and difficult to apply at a low density, except for select molecules with optical cycling transitions. An alternative approach to non-destructive detection suggested the use of Rydberg atoms.[11,12] It exploits, instead of driving molecular transitions by laser light, Förster resonant energy transfer (FRET), i.e., non-radiative energy exchange between the donor and acceptor mediated by the resonant dipole−dipole interaction.[13,14] Rydberg atoms are particularly well-suited to FRET as a result of their large dipole moment.[15,16] Rydberg states are readily prepared,[17,18] and the scaling of Rydberg transitions with the principal quantum number[19] allows for covering the microwave and terahertz spectral range, i.e., rotational transition frequencies in a large variety of molecules.[12] The basic feasibility of non-destructive detection of molecules via FRET with Rydberg atoms has been demonstrated for ammonia,[20] as has electric field control of the energy transfer.[20−22] The latter leverages the easy tunability of Rydberg energy levels as a result of their sensitivity to external fields.[23,24] Thanks to this tunability, it should be possible to use FRET not only to see whether a molecule is present or not but to actually infer the molecular state prior to the interaction. This would be an extremely useful tool for quantum technologies and studies of cold and ultracold chemistry but requires a description of the molecular structure beyond the popular two-level approximation.[4,5,12,20−22,25−27]

Here, we establish a first-principles-based theoretical framework for FRET in collisions of polar molecules with Rydberg atoms and predict electric-field-dependent cross sections with a full account of the interparticle dynamics. In an experiment, the cross sections will be obtained by measuring the final state of the Rydberg atom via, e.g., ionization as a function of the electric field. Whether the cross sections display well-resolved lines suitable for spectroscopy depends upon the key parameter governing a collision, the relative velocity. Well-resolved lines, in turn, allow for inferring the state of the molecule or molecular ensemble, as we show below. Such Rydberg spectroscopy of polar molecules only requires the existence of (near) resonant dipole transitions in the two particles.

Translational motion of the collision complex and internal degrees of freedom can be separated as a result of their different time and energy scales,[28] similar to the semi-classical impact parameter method.[29] The distance $\boldsymbol{r}_{\mathrm{mol}}(t)$ between the molecule and atomic core (cf. Figure 1a) is then a time-dependent parameter in the atom−molecule interaction. The Hamiltonian for the internal degrees of freedom is given by

$$\hat{H}(t) = \hat{H}_{\mathrm{ryd}} + \hat{V}_{\mathrm{ryd}}^{\mathrm{DC}} + \hat{H}_{\mathrm{mol}} + \hat{V}_{\mathrm{int}}(t) \tag{1}$$

Received: August 14, 2022
Accepted: November 8, 2022

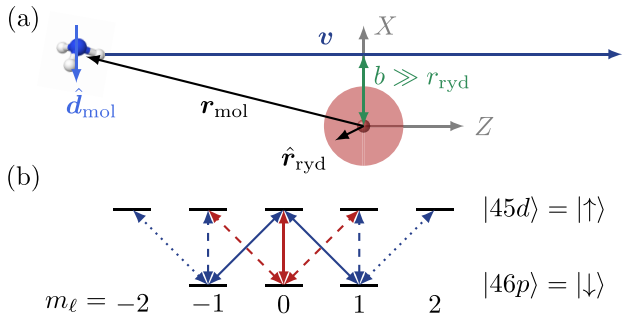

Figure 1. Collision-mediated Rydberg spectroscopy of polar molecules relies on the interaction of the molecular dipole moment (light blue arrow) with the electric field as a result of the charge distribution of the valence electron of the Rydberg atom (indicated by the shaded area). (a) Classical scattering trajectory (dark blue). (b) Relevant energy levels of the Rydberg atom, with all possible dipole transitions indicated by arrows.

where $\hat{V}_{\mathrm{ryd}}^{\mathrm{DC}}$ captures the Stark shifts in the Rydberg atom as a result of the direct current (DC) electric field[30] and $\hat{V}_{\mathrm{int}}(t)$ describes the interaction of the molecular electric dipole moment $\hat{\boldsymbol{d}}_{\mathrm{mol}}$, with the electric field arising from the charge distribution of the valence electron of the Rydberg atom. For sufficiently large distances between the atom and molecule, it is given by the dipole−dipole contribution

$$\hat{V}_{\mathrm{dd}}(t) = \frac{e}{4\pi\varepsilon_0}\left(\frac{\hat{\boldsymbol{d}}_{\mathrm{mol}}\hat{\boldsymbol{r}}_{\mathrm{ryd}}}{\boldsymbol{r}_{\mathrm{mol}}{}^{3}(t)} - \frac{3(\hat{\boldsymbol{d}}_{\mathrm{mol}}\boldsymbol{r}_{\mathrm{mol}}(t))(\hat{\boldsymbol{r}}_{\mathrm{ryd}}\boldsymbol{r}_{\mathrm{mol}}(t))}{\boldsymbol{r}_{\mathrm{mol}}{}^{5}(t)}\right) \tag{2}$$

where $\hat{\boldsymbol{r}}_{\mathrm{ryd}}$ is the position of the Rydberg electron. We assume the ensemble to be sufficiently dilute, such that a Rydberg atom interacts at most once with a molecule[28] and neglects any change of the molecular trajectory as a result of the interaction

$$\boldsymbol{r}_{\mathrm{mol}}(t) = v t \boldsymbol{e}_Z + b\boldsymbol{e}_X \tag{3}$$

with $v\boldsymbol{e}_Z$ is the velocity and b is the impact parameter, with the molecular beam direction chosen parallel to the DC field. We expect the best resolved spectra for this geometry as a result of symmetry; different orientations of the trajectory imply a dependence upon the azimuthal angle and, thus, an additional averaging. The Rydberg atom is assumed to change its state only as a result of FRET with the molecule. We denote the probability for this state change by $P_{\mathrm{ex}}^{\Psi_0}(\Delta,b)$ for a given initial state $|\Psi_0\rangle$ of the atom and molecule, with Δ being the energy mismatch between the molecular and atomic transition. To calculate $P_{\mathrm{ex}}^{\Psi_0}(\Delta,b)$, we solve the time-dependent Schrödinger equation with $\hat{H}(t)$, choosing initial and final times such that the atom and molecule are well-separated and $\hat{V}_{\mathrm{dd}}(t)$ is negligible. The corresponding cross section is obtained by integrating this probability over all impact parameters.

$$\sigma_{\Psi_0}(\Delta) = 2\pi\int_0^\infty \mathrm{d}b\, bP_{\mathrm{ex}}^{\Psi_0}(\Delta, b) \tag{4}$$

Electric field tunability of the cross section arises from tuning Δ via the Stark effect of the Rydberg atom. The semi-classical approximation is held down to a velocity of about $v = 0.1$ m/s.[28] This is also the lower limit for spectroscopy because, for even smaller velocities, the Rydberg atom will likely decay before the particles had enough time to interact.[28]

Motivated by recent experiments,[20,22] we consider FRET between Rydberg atoms and the inversion mode of ammonia. The molecular state can be written in terms of the vibrational inversion mode $|\nu^{\pm}\rangle$ and the symmetric top eigenstates $|JKM\rangle$.[28] Because rotational transition frequencies are large compared to the inversion splitting, it is sufficient to consider a single inversion doublet at a time, such that $|\nu^{\pm}JKM\rangle$, with $|\nu^{+}\rangle$ being the lowest and a symmetric sublevel and $|\nu^{-}\rangle$ being the second lowest and an antisymmetric sublevel of the inversion doublet for given J, K, and M. Coupling to other vibrational or electronic degrees of freedom is negligible. The inversion splitting depends upon J and K approximately as[31]

$$\omega_{\mathrm{inv}} = \omega_{\mathrm{inv}}^{0} - c_1(J(J+1) - K^2 + c_2K^2) \tag{5}$$

with constants $c_{1,2}$.[31] For fixed J and K, dipole transitions obey the selection rules $\nu^{\pm} \leftrightarrow \nu^{\mp}$ and $\Delta M = \pm 1$ or 0 (unless $M = 0 = M'$).

$\hat{H}_{\mathrm{ryd}}$ is represented in the spherical basis $|nl, m_l\rangle$ with principal quantum number n, angular quantum number l, and projection m_l. Assuming rubidium, levels with $l \leq 7$ are shifted as a result of the finite size of the ionic core,[32] by the quantum defect δ_{nlj}, which we approximate as $\delta_{nl} \approx \delta_{nl,j=l+1/2}$.[28] For low J and $K = J$, the inversion splitting of ammonia is matched by transitions between $|46p, m_l\rangle \equiv |\downarrow, m_l\rangle$ and $|45d, m_l'\rangle \equiv |\uparrow, m_l'\rangle$ (cf. Figure 1b). For $J = K = 1$, the energy mismatch between the atomic and molecular transitions is shown in Figure 2a as a function of the DC field strength. It vanishes at different field strengths for transitions involving different m_l. This is at the core of the suggested spectroscopy.

We consider two different scenarios, both of which can be realized with existing experimental setups. In the first scenario, we assume the molecule to be prepared in a single rotational energy level, for example, in an experiment with a suitable (e.g., quadrupole) guide or Stark decelerator.[33−35] In the second scenario, we consider molecules in essentially arbitrary rotational states, taking a thermal state as example, and show that this state can be inferred from the measurements. The two scenarios differ in the number of state-to-state cross sections that have to be averaged when predicting the outcome of an experiment. Both rely on FRET between the atom and molecule and both assume state-resolved detection of the Rydberg atom after the collision.

Starting with the first scenario of molecules in a single rotational level, we assume $J = K = 1$ for the molecule and the Rydberg atom in one of the states $|\downarrow, m_l\rangle$ with $m_l = 0$ or ± 1. The choice of m_l is easily ensured by a suitable laser polarization in the Rydberg state preparation. Because the energy transfer is resonant, it is sufficient to consider only the upper inversion level for the molecule, $|\nu^{-}, M\rangle$ with $M = 0$ or ± 1. The state-to-state cross sections for all possible initial states are shown as a function of the DC field strength for three relative velocities in panels b−d of Figure 2, with resonances indicated by vertical lines. As the velocity increases, the cross section peaks increase in width and decrease in amplitude. For dipole−dipole transitions, the maximum of the cross section and its line width scale as[12]

$$\max(\sigma) \propto d_{\mathrm{mol}}/v, \qquad \Delta \propto v^{3/2}/\sqrt{d_{\mathrm{mol}}} \tag{6}$$

with $d_{\mathrm{mol}} \propto K/\sqrt{J(J+1)}$ for the considered transition in symmetric top molecules.[36]

Molecules in a molecular beam experiment are randomly oriented, corresponding to all M states being populated. We thus consider two M-averaged cross sections, for $m_l = 0$ and 1

https://doi.org/10.1021/acs.jpclett.2c02521
J. Phys. Chem. Lett. 2022, 13, 10728−10733

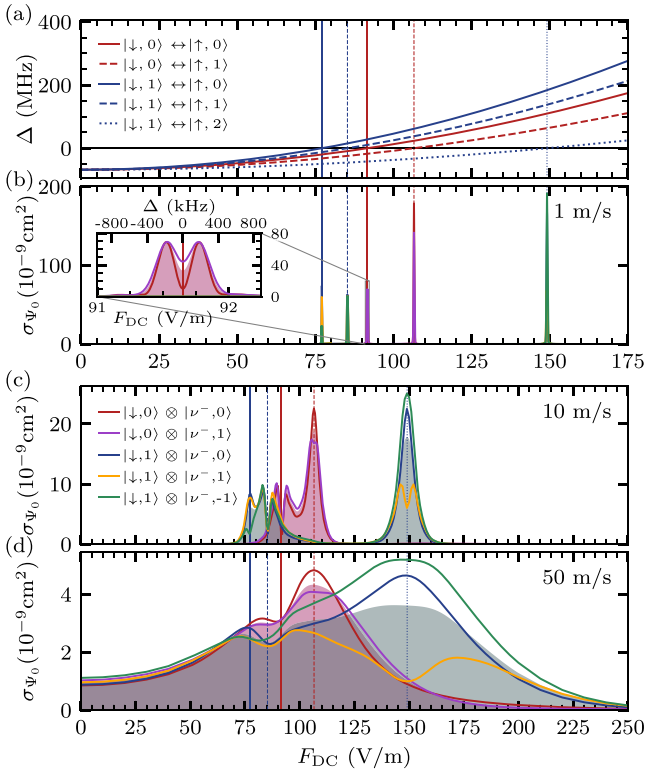

Figure 2. Electric field control of collisions between molecules prepared in a single rotational energy level (here, $J = 1 = K$) and Rydberg atoms. (a) Energy mismatch Δ between the inversion mode of ammonia and the Rydberg transitions shown in Figure 1b. Vertical lines indicate resonances. (b–d) State-to-state cross sections for different initial states (indicated by the line color) and velocities (panels). Red (green) shaded areas show cross sections averaged over degenerate initial molecular states with the atom in $|\downarrow, 0\rangle$ ($|\downarrow, 1\rangle$). Note the different scales of the x and y axes.

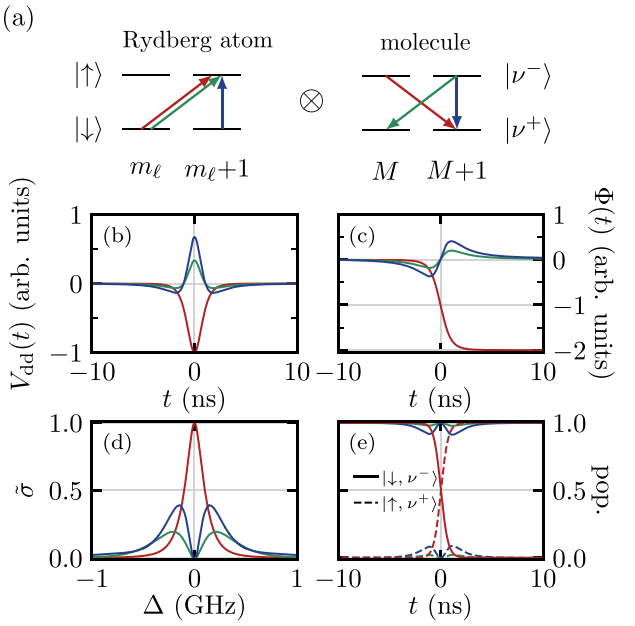

Figure 3. (a) Types of transitions in two TLS as a result of dipole–dipole coupling and (b–e) their behavior during the collision: (b) interaction strength $\hat{V}_{dd}(t)$ scaled to a maximal absolute value of 1, (c) its integrated value $\Phi(t)$, (d) normalized cross section $\tilde{\sigma} = \sigma/\sigma_{max}$ as a function of the energy mismatch Δ (with $\sigma_{max} = 1.7 \times 10^{-9}$ cm^2), and (e) exemplary time evolution at resonance.

(shaded areas in panels b–d of Figure 2): At low velocities, the peaks do not overlap (Figure 2b) and are also clearly distinguishable for higher velocities (Figure 2c). While the resolution of single transitions is hampered at an increasing velocity, the two M-averaged cross sections continue to be distinguishable up until about $v = 50$ m/s (Figure 2c). In particular, the two resonances occurring at the largest field strengths, corresponding to $|\downarrow, m_l = 0; \nu^-, M\rangle \leftrightarrow |\uparrow, m_l = 1; \nu^+, M'\rangle$ for the dashed red and $|\downarrow, m_l = 1; \nu^-, M\rangle \leftrightarrow |\uparrow, m_l = 2; \nu^+, M'\rangle$ for the dotted blue vertical lines, can be resolved. It is thus possible to deduce from the recorded cross sections the molecular energy splitting and, hence, the rotational level. At higher velocities, this is no longer the case.

The peak heights in panels b–d of Figure 2 imply that an effective volume of 2×10^{-9} cm^3 is probed by one Rydberg atom, assuming an interaction time of 100 μs. This suggests a fully saturated signal at a molecular density of 5×10^8 cm^{-3}. In experiments, the molecular signal has to be discriminated against the background, mainly as a result of Rydberg transitions caused by blackbody radiation.[20] Given the cross sections in panels b–d of Figure 2, this should be possible for densities as low as 10^5 cm^{-3}.[28]

Various lineshapes are observed in panels b and c of Figure 2, even in the M-averaged case. For example, if the Rydberg atom starts in $m_l = 0$ (vertical red lines), the cross section around 107 V/m (dashed) is Lorentzian but displays a clear dip around 92 V/m (solid, see the inset). We now show that it is the time dependence of the interaction (eq 2) as a result of the collision that is reflected in the lineshape.

The selection rules allow for three types of FRET transitions (cf. Figure 3a), which we term criss-cross (red) and linear (blue) and diagonal (green) flip-flop. To analyze each type separately, we reduce the Hilbert space of the atom and molecule to only two states each, the states connected by the respective transitions in Figure 3a. Then, there is only a single matrix element for the interaction, $V_{dd}(t) = \langle \downarrow, m_l; \nu^-, M|\hat{V}_{dd}(t)|\uparrow, m_l'; \nu^+, M'\rangle$, shown in Figure 3b for $v = 100$ m/s and $b = 160$ nm. It is symmetric as a function of time around $t = 0$, where the two particles are closest to each other and $V_{dd}(t)$ takes its extremal value. The two coupled two-level systems (TLS) accumulate a relative phase, which in the resonant case is simply given by $\Phi(t) = \int_{-\infty}^{t} V_{dd}(t')dt'$, shown in Figure 3c. For the criss-cross transitions (red lines), $V_{dd}(t)$ is always negative, $\Phi(t)$ thus decreases monotonically, the two TLS exchange their excitation perfectly (Figure 3e), and the TLS cross section displays a Lorentzian peak (Figure 3d). For flip-flop transitions (green and blue lines in panels b–e of Figure 3), the non-Lorentzian lineshapes are rationalized by the different time evolutions of $V_{dd}(t)$ with two changes of sign. Phase accumulation is then non-monotonic, and most importantly, the phase equals zero at $t = 0$. This causes the TLS to return to their initial states (cf. Figure 3e), resulting in a vanishing cross section at resonance. Shifting the transitions away from resonance breaks the symmetry in the time evolution of $V_{dd}(t)$, resulting in a non-vanishing accumulated phase and cross section. This behavior is observed for both linear and

https://doi.org/10.1021/acs.jpclett.2c02521
J. Phys. Chem. Lett. 2022, 13, 10728–10733

diagonal flip-flop transitions because only the overall strength of their coupling differs.

While the cross sections in Figure 2 arise from more complex dynamics than that of two coupled TLS, the peaks resemble lineshapes as seen in Figure 3d. For example, the peak at 107 V/m for the initial state $|\downarrow, m_l = 0\rangle \otimes |\nu^-, M = 1\rangle$ (purple line) is Lorentzian, suggesting a criss-cross transition, where both m_l and M change by one. Indeed, we numerically find the transition to $|\uparrow, m_l = -1\rangle \otimes |\nu^+, M = 0\rangle$ to be dominant. In contrast, around 92 V/m, the peak shows a deep dip as a result of a flip-flop transition to $|\uparrow, m_l = 0\rangle \otimes |\nu^+, M = 1\rangle$. Note that the state-to-state cross sections in Figure 2 do not vanish entirely at resonance because our model includes all m_l/M sublevels. Repeating the analysis for all initial states in Figure 2, we find all resonances to be dominated by one type of transition.[28] The electric-field-controlled cross sections thus reveal whether a criss-cross or flip-flop transition is at the core of a resonance.

We now discuss the second scenario, showing how to employ Rydberg spectroscopy to infer the population of molecular states. Figure 4 illustrates the working principle,

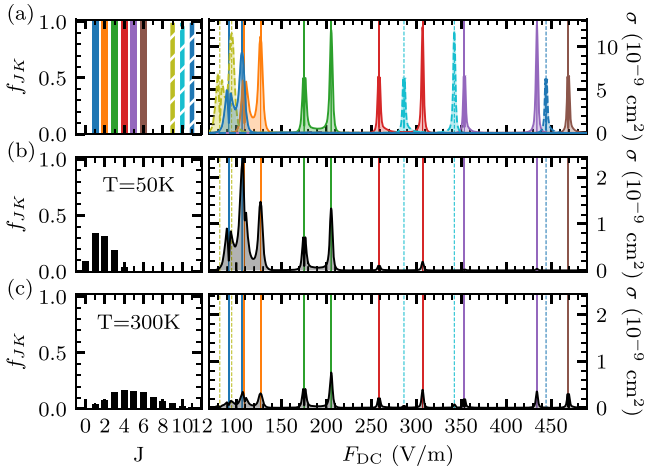

Figure 4. (a) Rydberg spectroscopy with M-averaged cross sections shown on the right (for v = 10 m/s and m_l = 0) and relative populations of the rotational states shown on the left for single rotational levels and (b and c) thermal ensembles at rotational temperatures of 50 and 300 K, respectively. The vertical lines indicate resonances; solid lines correspond to $K = J$; and dashed lines correspond to $K = J - 1$ (other molecular transitions are far off-resonant).

correlating rotational states with peaks in the cross section. The dependence of the M-averaged cross section on the rotational quantum numbers J and K, shown in Figure 4a, can be observed as a function of the DC field strength as a result of dependence of the inversion splitting on J and K (cf. eq 5). Figure 4 focuses on states with the Rydberg atom initially in $m_l = 0$ (for $m_l = 1$, cf. ref 28) and molecules in $J \leq 11$, which have an inversion splitting near resonant to the Rydberg transition at the considered electric field strengths and temperatures. The cross sections in Figure 4a display a sequence of resonances, similar to Figure 2b, with the position and height of the peaks depending upon K, in perfect agreement with the scaling of eq 6. When a thermal ensemble is considered, the cross sections are obtained by averaging over all states in the ensemble (cf. panels b and c of Figure 4). The occupation of the rotational states is then given by $f_{JK}(T) = g/\mathcal{N}e^{-E_{JK}/k_BT}$, with T being the temperature, $\mathcal{N}$ being a normalization factor, and g being the statistical weight of the state.[28] At very low temperatures, $T \leq 10$ K, the $J = K = 1$ contribution dominates, leading to a similar pattern as shown in Figure 2b. At higher rotational temperatures (panels b and c of Figure 4), an increasing number of rotational states contributes. For a relative velocity of v = 10 m/s, as shown in Figure 4, the resonances are easily resolved and assigned to the different rotational states. The resonances for J = 1 and 2 between 70 and 140 V/m are the hardest to resolve, but Figure 2 shows that this is possible until at least 50 m/s. Provided that the velocity is sufficiently low, measurement of the cross section as a function of the electric field strength thus allows for inferring the rotational state composition of the molecular ensemble from the position and height of the peaks. An explicit example is worked out in ref 28. To determine the composition of states with other K values, simply a different Rydberg transition has to be selected, e.g., $|47p, m_l\rangle$ to $|46d, m_l'\rangle$.

In summary, we have derived the principles of a collision-mediated, non-destructive spectroscopy of polar molecules, using a complete dynamical description from first principles. Instead of the light−matter interaction, the spectroscopy is based on the resonant dipole−dipole interaction with Rydberg atoms. Taking ammonia and rubidium as an example, we have shown that the electric field control of the cross sections allows for inferring the relative population of rotational states for velocities below 100 m/s. The lineshape reveals the dominant type of FRET-induced transition. For very low velocities, of the order of 1 m/s, line widths below 1 MHz will be obtained. The considered velocities between 100 and 1 m/s cover the range relevant for application of the suggested spectroscopy in cold reaction dynamics and quantum technologies. A key advantage of Rydberg atom-enabled spectroscopy is the ability to measure spectra for extremely low molecular density. Detection of single molecules in optical tweezers or at molecular densities as low as 10^5 cm^{-3} seems realistic.

Our example of ammonia and rubidium is easily carried over to other atomic and molecular species. Exchanging rubidium by helium,[22] for instance, mainly reduces the quantum defects, rendering the isolation of a suitable dipole−dipole transition from neighboring (possibly higher order) transitions somewhat more difficult. When ammonia is replaced by other polar molecules, purely rotational transitions can be used instead of the inversion mode.[12] A further prospect is to probe transitions governed by higher order terms in the multipole expansion; this simply requires a suitable choice of Rydberg levels. A method for state-resolved non-destructive detection of polar molecules addresses an essential need for their application in quantum technologies and cold reaction dynamics studies and establishes Rydberg atoms as a versatile addition to the quantum control toolbox for cold and ultracold molecules.[4,5,25−27]

■ ASSOCIATED CONTENT

Supporting Information

The Supporting Information is available free of charge at https://pubs.acs.org/doi/10.1021/acs.jpclett.2c02521.

Details of the molecular model, details of the model for the Rydberg atom, validity of the model, approximation of necessary molecular densities, detailed analysis of the peak structure in the electric field-controlled cross

https://doi.org/10.1021/acs.jpclett.2c02521
J. Phys. Chem. Lett. 2022, 13, 10728−10733

section of Figure 2, molecules in an ensemble of rotational states for m_l = 1, and fitting the relative populations from measured cross sections (PDF)

Transparent Peer Review report available (PDF)

AUTHOR INFORMATION

Corresponding Author

Christiane P. Koch − *Dahlem Center for Complex Quantum Systems and Fachbereich Physik, Freie Universität Berlin, 14195 Berlin, Germany*; orcid.org/0000-0001-6285-5766; Email: christiane.koch@fu-berlin.de

Authors

Sabrina Patsch − *Dahlem Center for Complex Quantum Systems and Fachbereich Physik, Freie Universität Berlin, 14195 Berlin, Germany*

Martin Zeppenfeld − *Max-Planck-Institut für Quantenoptik, 85748 Garching, Germany*

Complete contact information is available at: https://pubs.acs.org/10.1021/acs.jpclett.2c02521

Notes

The authors declare no competing financial interest.

ACKNOWLEDGMENTS

The authors thank Ed Narevicius, Ronnie Kosloff, and Melanie Schnell for insightful discussions. Financial support from the Studienstiftung des deutschen Volkes e.V. and the Deutsche Forschungsgemeinschaft via the Priority Programme GiRyd (KO 2301/14-1 Grant 428456483) and Grant ZE 1096/2-1 is gratefully acknowledged.

REFERENCES

(1) Hutzler, N. R. Polyatomic molecules as quantum sensors for fundamental physics. *Quantum Sci. Technol.* **2020**, *5*, 044011.

(2) Mitra, D.; Leung, K. H.; Zelevinsky, T. Quantum control of molecules for fundamental physics. *Phys. Rev. A* **2022**, *105*, 040101.

(3) Albert, V. V.; Covey, J. P.; Preskill, J. Robust Encoding of a Qubit in a Molecule. *Phys. Rev. X* **2020**, *10*, 031050.

(4) Wang, K.; Williams, C. P.; Picard, L. R. B.; Yao, N. Y.; Ni, K.-K. Enriching the quantum toolbox of ultracold molecules with Rydberg atoms. *arXiv.org, e-Print Arch., At. Phys.* **2022**, arXiv:2204.05293.

(5) Zhang, C.; Tarbutt, M. R. Quantum computation in a hybrid array of molecules and Rydberg atoms. *arXiv.org, e-Print Arch., Quantum Phys.* **2022**, arXiv:2204.04276.

(6) *Cold Chemistry*; Dulieu, O., Osterwalder, A., Eds.; The Royal Society of Chemistry: London, U.K., 2018; Theoretical and Computational Chemistry Series.

(7) Shuman, E. S.; Barry, J. F.; Glenn, D. R.; DeMille, D. Radiative force from optical cycling on a diatomic molecule. *Phys. Rev. Lett.* **2009**, *103*, 223001.

(8) Wang, D.; Neyenhuis, B.; de Miranda, M. H.; Ni, K. K.; Ospelkaus, S.; Jin, D. S.; Ye, J. Direct absorption imaging of ultracold polar molecules. *Phys. Rev. A* **2010**, *81*, No. 061404(R).

(9) Cheuk, L. W.; Anderegg, L.; Augenbraun, B. L.; Bao, Y.; Burchesky, S.; Ketterle, W.; Doyle, J. M. Λ-Enhanced Imaging of Molecules in an Optical Trap. *Phys. Rev. Lett.* **2018**, *121*, 083201.

(10) Shaw, J. C.; Schnaubelt, J. C.; McCarron, D. J. Resonance Raman optical cycling for high-fidelity fluorescence detection of molecules. *Phys. Rev. Res.* **2021**, *3*, L042041.

(11) Kuznetsova, E.; Rittenhouse, S. T.; Sadeghpour, H. R.; Yelin, S. F. Rydberg-atom-mediated nondestructive readout of collective rotational states in polar-molecule arrays. *Phys. Rev. A* **2016**, *94*, 032325.

(12) Zeppenfeld, M. Nondestructive detection of polar molecules via Rydberg atoms. *EPL* **2017**, *118*, 13002.

(13) Förster, T. Zwischenmolekulare Energiewanderung und Fluoreszenz. *Ann. Phys.* **1948**, *437*, 55−75.

(14) Andrews, D. L.; Demidov, A. A.*Resonance Energy Transfer*; Wiley: Hoboken, NJ, 1999.

(15) Safinya, K. A.; Delpech, J. F.; Gounand, F.; Sandner, W.; Gallagher, T. F. Resonant Rydberg-Atom-Rydberg-Atom Collisions. *Phys. Rev. Lett.* **1981**, *47*, 405−408.

(16) Ravets, S.; Labuhn, H.; Barredo, D.; Béguin, L.; Lahaye, T.; Browaeys, A. Coherent dipole−dipole coupling between two single Rydberg atoms at an electrically-tuned Förster resonance. *Nat. Phys.* **2014**, *10*, 914−917.

(17) Haroche, S.; Raimond, J.-M.*Exploring the Quantum. Atoms, Cavities, and Photons*; Oxford University Press: New York, 2006.

(18) Larrouy, A.; Patsch, S.; Richaud, R.; Raimond, J.-M.; Brune, M.; Koch, C. P.; Gleyzes, S. Fast Navigation in a Large Hilbert Space Using Quantum Optimal Control. *Phys. Rev. X* **2020**, *10*, 021058.

(19) Šibalić, N.; Adams, C. S.*Rydberg Physics*; IOP Publishing: Bristol, U.K., 2018; pp 1−27.

(20) Jarisch, F.; Zeppenfeld, M. State resolved investigation of Förster resonant energy transfer in collisions between polar molecules and Rydberg atoms. *New J. Phys.* **2018**, *20*, 113044.

(21) Zhelyazkova, V.; Hogan, S. D. Electrically tuned Förster resonances in collisions of NH_3 with Rydberg He atoms. *Phys. Rev. A* **2017**, *95*, 042710.

(22) Gawlas, K.; Hogan, S. D. Rydberg-State-Resolved Resonant Energy Transfer in Cold Electric-Field-Controlled Intrabeam Collisions of NH_3 with Rydberg He Atoms. *J. Phys. Chem. Lett.* **2020**, *11*, 83−87.

(23) Facon, A.; Dietsche, E.-K.; Grosso, D.; Haroche, S.; Raimond, J.-M.; Brune, M.; Gleyzes, S. A sensitive electrometer based on a Rydberg atom in a Schrödinger-cat state. *Nature* **2016**, *535*, 262−265.

(24) Adams, C. S.; Pritchard, J. D.; Shaffer, J. P. Rydberg atom quantum technologies. *J. Phys. B* **2019**, *53*, 012002.

(25) Kuznetsova, E.; Rittenhouse, S. T.; Beterov, I. I.; Scully, M. O.; Yelin, S. F.; Sadeghpour, H. R. Effective spin−spin interactions in bilayers of Rydberg atoms and polar molecules. *Phys. Rev. A* **2018**, *98*, 043609.

(26) Huber, S. D.; Büchler, H. P. Dipole-Interaction-Mediated Laser Cooling of Polar Molecules to Ultracold Temperatures. *Phys. Rev. Lett.* **2012**, *108*, 193006.

(27) Zhao, B.; Glaetzle, A. W.; Pupillo, G.; Zoller, P. Atomic Rydberg Reservoirs for Polar Molecules. *Phys. Rev. Lett.* **2012**, *108*, 193007.

(28) See the Supporting Information for technical details, which includes refs 37−40.

(29) Beigman, I.; Lebedev, V. Collision theory of Rydberg atoms with neutral and charged particles. *Phys. Rep.* **1995**, *250*, 95−328.

(30) The Stark effect of the molecule is negligible at the relevant field strengths.[31]

(31) Townes, C. H.; Schawlow, A. L.*Microwave Spectroscopy*; Dover Publications, Inc.: New York, 1975.

(32) Gallagher, T. F.*Rydberg Atoms*; Cambridge University Press: Cambridge, U.K., 1994; Cambridge Monographs on Atomic, Molecular, and Chemical Physics.

(33) Petitjean, L.; Gounand, F.; Fournier, P. R. Collisions of rubidium Rydberg-state atoms with ammonia. *Phys. Rev. A* **1986**, *33*, 143.

(34) Bethlem, H. L.; Crompvoets, F. M. H.; Jongma, R. T.; van de Meerakker, S. Y. T.; Meijer, G. Deceleration and trapping of ammonia using time-varying electric fields. *Phys. Rev. A* **2002**, *65*, 053416.

(35) Chervenkov, S.; Wu, X.; Bayerl, J.; Rohlfes, A.; Gantner, T.; Zeppenfeld, M.; Rempe, G. Continuous centrifuge decelerator for polar molecules. *Phys. Rev. Lett.* **2014**, *112*, 013001.

(36) Kroto, H. W.*Molecular Rotation Spectra*; John Wiley and Sons, Ltd.: New York, 1975.

(37) Šibalić, N.; Pritchard, J. D.; Adams, C. S.; Weatherill, K. J. ARC: An open-source library for calculating properties of alkali Rydberg atoms. *Comput. Phys. Commun.* **2017**, *220*, 319−331.
(38) Meschede, D. Centimeter-wave spectroscopy of highly excited rubidium atoms. *J. Opt. Soc. Am. B* **1987**, *4*, 413−419.
(39) Han, J.; Jamil, Y.; Norum, D. V. L.; Tanner, P. J.; Gallagher, T. F. Rb *nf* quantum defects from millimeter-wave spectroscopy of cold ^{85}Rb Rydberg atoms. *Phys. Rev. A* **2006**, *74*, 054502.
(40) Nussenzveig, P.Mesures de champs au niveau du photon par interférométrie atomique. Ph.D. Thesis, Université Pierre et Marie Curie, Paris, France, 1994.

https://doi.org/10.1021/acs.jpclett.2c02521
J. Phys. Chem. Lett. 2022, 13, 10728−10733